Nanotechnology Perceptions
ISSN 1660-6795
www.nano-ntp.com

The confinement effect of the shell on the axial strength of thin wall circular section concrete filled steel tubes

Bekalu Gashu Alemu[1], K.Srinivasa Rao[2]

[1]Dept. of Civil Engineering, AUCE, Visakhapatnam, India
[2]Professor, Dept. of Civil Engineering, AUCE, Visakhapatnam, India

Abstract

This study uses experimental, numerical, and finite element (FE) analysis to demonstrate the vertical load-carrying capacity of thin-walled circular section concrete-filled steel tubes (TCSCFST) with core concrete and thin-walled unfilled steel tubes (UF). According to the experimental results, the average load factor of the TCSCFST is N_E = 4.92 and N_E = 5.52, respectively, based on the theoretical value estimated by Eurocode-4, EN 1994-1-1 (2004) part 1-1 for specimens with heights of 320 and 315 mm. Additionally, according to the experimental testing results, the TCSCFS's axial bearing capacity is improved by an average load factor of N_A = 4.92 and N_A = 5.51 from the theoretical value calculated for 320 and 315 mm height using the American Institute of Steel Construction (AISC) design code. The experiment also reveals that, compared to the theoretical value calculated using the AISC design code, the core concrete's axial bearing capacity rises by a load factor of N_{CA} = 26.68 and N_{CA} = 34.01 for 320 mm and 315 mm height specimens, respectively. In order to know whether a core concrete or shell is highly enhanced by the confinement effect, a FE analysis investigation on TCSCFS and UF steel tube is undertaken. The FE analysis result shows that the axial bearing capacity of the core concrete is increased by a load factor of $N_{CF,E}$ = 13.63 and $N_{CF,E}$ = 13.10 for 320 and 315 mm height specimens, respectively, from the numerical value estimated by Eurocode-4, EN 1994-1-1 (2004) part 1-1. In addition, the axial bearing capacity of the core concrete is determined by FE analysis and also increases by a load factor of $N_{CF,A}$ = 21.40 and $N_{CF,A}$ = 20.38 for 320 and 315 mm height specimens, respectively, from the numerical value estimated by AISC. As per the study, the confinement effect of steel enhances the axial bearing capacity of the inner concrete and the shell; however, Eurocode-4, EN 1994-1-1 (2004) Part 1-1, and AISC design codes show more conservative values than the experimental and finite element analysis results.

Keywords: TWCSCFST, UF steel tubes, core concrete, FE analysis, axial load, numerical result

1. Introduction

Concrete and steel have recently been combined to create a hybrid building material. One of the hybrid building materials used to construct long-span bridges and high-rise structures is concrete-filled steel tube (CFST). The benefits of CFST include lower construction costs, increased rigidity, fire resistance, formwork functionality, and shorter building times. When the steel tubes yield at excessive longitudinal stress and their transverse confinement to the interior concrete is severely weakened, the drawback of CFST in beam-to-column connections becomes more complex (Yan Xiao et al.)) [1]. The performance of concentrically loaded thick wall concrete-filled steel tubes was examined in a number of studies using different shell diameters, thicknesses, heights, core concretes, shapes, and ties (Kwan A. K. H., Ouyang Y., 2017 [2]; Hu et al., 2003 [3]; Jian Cai and Yue-Ling Long, 2007 [4]; Lin-Hai Han et al., 2007 [5]. The study indicates that the axial bearing capacity of thick wall steel tubes is well-served by CFST, which diminishes as the diameter-to-

thickness ratio rises. It also demonstrates that the circular section's confinement action is superior to that of the square section. An experimental investigation on the seismic shock resistance of concrete-filled steel tubes was conducted by Yan Xiao and al., 2005 [6], who came to the conclusion that CFST is exceptional in seismic resistance. Determining the CFST's confinement behaviour, a critical feature that contributes significantly to its high axial bearing capacity, is difficult phenomena. Research revealed that the steel's confinement effect cannot be predicted using the same numerical formula as it was outlined in AISC and Eurocode 4. The axial strength of thick wall box CFST columns was predicted using a simplified and modified method by (Ammar Abbas Ali and Nazar Jabbar Abbas, 2021 [7]). To investigate the confinement effect of a thick wall circular section concrete filled steel tube, researchers (Hoang An Le, 2023 [8], Liusheng He et al., 2017 [9]; Zhi-wu Yua et al., 2007 [10]; Li Bing et al., 2001 [11]; Farid Abed et al., 2012 [12]) conducted an experimental study. The results were compared with Eurocode 4 (EC4) and (AISC). The investigation found that the real bearing capacity of CFST is significantly different from both ASC and Eurocode 4 (EC4). The strength of the bond between the slave and the shell was also impacted by temperature, according to earlier research. According to the study of Zhong Tao et al. (2010) [13], the ability of shell and slave to bind decreases as the temperature rises and diminish the axial capacity of CFST. The axial bearing capacity of the CFST was also affected by a layer of steel tube. A higher axial load can be supported by steel tubes filled with double-skin concrete than by steel tubes filled with single-skin concrete, according to Qing Quan Liang (2017) [14]). Utilizing Artificial Neural Networks (ANN), a finite element analysis tool, Yansheng Du et al. (2017) [15] built a model utilizing the previous experimental data, and the results were nearly the same as the experimental data. This study investigates circular, thin-walled steel tubes filled with M20 concrete and left unfilled under concentric load. The tubes have an outside diameter of 48.17 mm and a thickness of 1 mm. The experimental results of the TCSCFST are modelled using ABAQUS software.

2. Materials and Methods

2.1. Experimental investigations

2.1.1. Test specimens

To complete this study, a total of 12 test specimens are created using steel tubes with thin walls and circular sections. Nine of the twelve specimens are filled with concrete, while the other three are left empty. The specimens' outside diameter is 48.17 mm, and they measure 315 and 320 mm in height and 1 mm in thickness. Digital callipers are used to repeatedly measure the steel tubes' outer diameter and wall thickness in order to verify their precise measurements. A 1 mm thick sheet plate is used to seal off one end of the specimens to stop concrete from slipping while it is being cast and compacted. A 20 mm wide strip taken from thin-walled steel tubes is subjected to a tensile test in accordance with IS 1608:2005 [16] guidelines provided to ascertain the mechanical properties of the shell.The tensile test result indicated that the steel has a yield strength of 300 MPa and Young's modulus of (E_s) nearly 200,000 MPa. The circular section steel tubes are filled with M20 core concrete grade and compacted with a table vibrator. The variables considered in the study are the grade of core concrete, the aspect ratio (L/D), the axial load level for TCSCFST specimens estimated by Eurocode-4, EN 1994-1-1 (2004) Part 1-1 and AISC code of design, and the axial load level for core concrete specimens. The physical behavior of the samples are indicated in Table 1, and the outline of UF and TCSCFST test samples is shown in Fig. 1.

$$N_E = \frac{p_{\text{exp.}}}{p_{u,E}} \quad (1)$$

$$N_A = \frac{p_{\text{exp.}}}{p_{u,A}} \quad (2)$$

$$N_F = \frac{p_{\text{exp.}}}{p_{u,FE}} \quad (3)$$

$$N_{CE} = \frac{p_{\text{exp.}} - p_{\text{exp.}UF}}{p_{u,E} - p_{u,UF,E}} \quad (4)$$

$$N_{CA} = \frac{p_{\text{exp.}} - p_{\text{exp.}UF}}{p_{u,A} - p_{u,UF,A}} \quad (5)$$

$$N_{CF,E} = \frac{p_{FE} - p_{UF,F}}{p_{u,E} - p_{u,UF,E}} \quad (6)$$

$$N_{CF,A} = \frac{p_{FE} - p_{UF,F}}{p_{u,A} - p_{u,UF,A}} \quad (7)$$

Where N_E is load factors of TCSCFST as per Eurocode -4, EN 1994-1-1 (2004) part 1-1, $p_{\text{exp.}}$ is an experimental load of TCSCFST, $P_{u,E}$ is the numerical value of the TCSCFST calculated by Eurocode-4, EN 1994-1-1 (2004) part 1-1, N_A is load factors of TCSCFST based on AISC, $p_{u,A}$ is the numerical value of the TCSCFST calculated by AISC, N_F is load factors of TCSCFST based on FE analysis, $P_{u,FE}$ is the numerical value of the TCSCFST defined by FE analysis, N_{CE} is load factors of core concrete based on Eurocode -4, EN 1994-1-1 (2004) part 1-1, $p_{\text{exp.}UF}$ is experimental value of UF steel tubes, $P_{u,UF,E}$ is the numerical value of the UF steel tube calculated by Eurocode-4, EN 1994-1-1 (2004) part 1-1, N_{CA} is load factors of core concrete based on AISC, $P_{UF,F}$ is the numerical value of the UF steel tube calculated by FE analysis, $P_{u,UF,A}$ is the numerical value of the UF steel tube calculated by AISC, $N_{CF,E}$ is a finite element load factor of core concrete based Eurocode -4, EN 1994-1-1 (2004) part 1-1, $P_{u,UF,E}$ is the numerical value of the UF steel tube calculated by Eurocode-4, EN 1994-1-1 (2004) part 1-1, $N_{CF,A}$ is a finite element load factor of core concrete based AISC.

Table 1 Physical properties of thin wall circular section steel tube specimens

Specimens	Height of specimens (mm)	Total number of specimens	Thickness of steel tubes (mm)	Yield strength of steel tubes (Mpa)	Young's modulus of steel tubes (Mpa)
Thin wall Circular section steel tubes	315	7	1	300	2,00,000.00
	320	5			

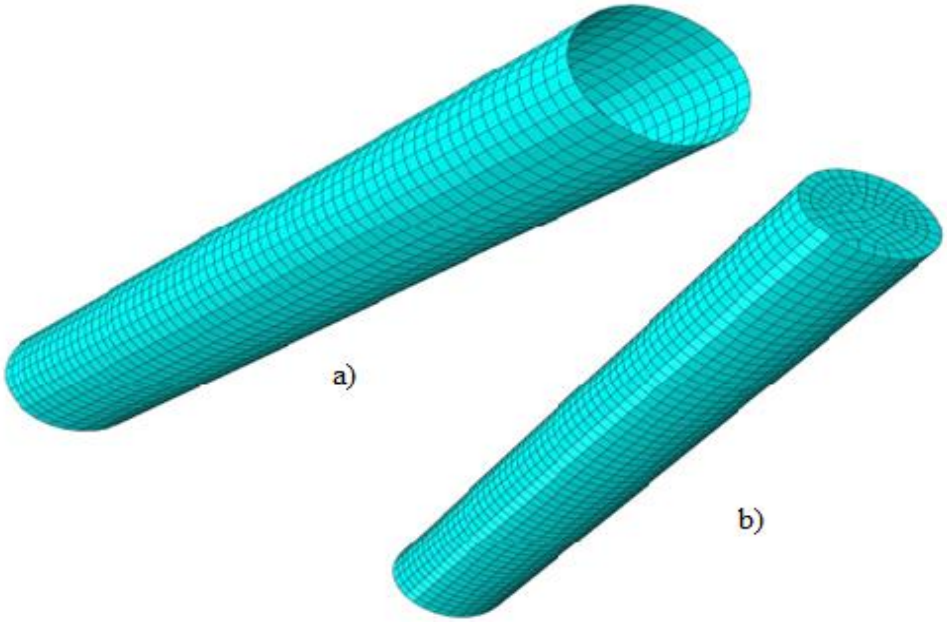

a) UF b) TCSCFST

Fig. 1 Unfilled steel tubes and TCSCFST layout

2.1.2. Mix design of core concrete

Various tests are carried out in order to define the physical properties of the main components of concrete, including gradation, water absorption, organic contaminants, and specific gravity. According to IS 10262:2009 [17], the quantity of core concrete ingredients needed for M20 core concrete are calculated. The cement grade utilized for the core concrete is OPC 42.5. Figure 2 displays the fine and coarse aggregate used in the experiment, while Table 2 displays the mix proportions of core concrete, water cement ratio (W/C), and slump values during casting.

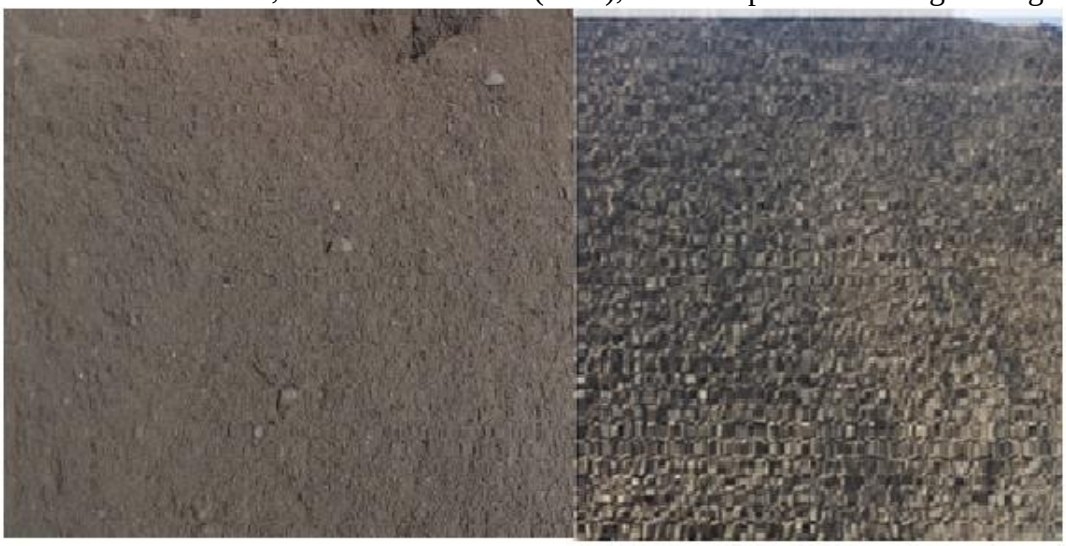

a) Fine aggregate **b)Coasrse aggregate**

Fig. 2 Coarse and fine aggregate

Table 2 Mix proportions of core concrete

Grade of core concrete	Cement (kg/m^3)	Fine aggregate (kg/m^3)	Coarse aggregate (kg/m^3)	Water (l/m^3)	W/C	Slump (mm)	Mix proportions
M20	329	787	1115	233	0.5	36	1:3.29:3.51

2.1.3. Casting and testing of core concrete specimens

In the study, the cube compressive capacity of the slaves is tested at 7, 14, and 28 days. The compressive capacity and target mean strength of cube specimens at 7, 14, and 28 days for the slaves are shown in Table 3.

Table 3 Compressive capacity of a slave at 7, 14, and 28 days and its target strength

S.No.	Grade of concrete	Compressive strength in N/mm^2 at			Target strength N/mm^2
		7 days	14 days	28 days	
1	M20	17.61	24.04	25.79	26.60

2.1.4. Testing of TCSCFST

The TCSCFST is casted, cured, and tested after 28 days. The end of the specimens is supported at the top and bottom of the concentric loading frame compressive testing machine, considering that only axial displacement is allowed. Loading is applied up to the specimen collapses due to cracking, local buckling, or global bending. During testing, once the axial capacity of TCSCFST reached its ultimate value, even though time increased slowly, the display unit of the compressive testing machine ceased to show any more incremental load value.

2.2. Numerical value of TWCSCFST as per European and American design codes

In this study, the numerical compressive capacity of the TCSCFST specimens was estimated by the Eurocode-4, EN 1994-1-1 (2004) part 1-1 [18] and AISC, March 9, 2005 [19].

2.2.1. According to the Eurocode – 4, EN 1994-1-1 (2004) part 1-1, the design compressive strength of the specimens can be calculated as:

$$n_{\mathrm{pl},rd} = \Psi_s s_{\mathrm{a}}\ \mathrm{f}_a + c_{\mathrm{c}}\ \mathrm{f}_{\mathrm{d}}\,(1+\Psi_{cc}\frac{(\mathrm{t})}{\mathrm{D}}\frac{(f_{\mathrm{y}})}{f_{\mathrm{k}}}) \qquad (8)$$

Where $n_{\mathrm{pl},rd}$ the plastic resistance to compression, ψs and ψ cc are the confinement ratios for the shell and slave respectively, S_{a} and C_{a} are the areas of the shell and slave respectively, D is the outer diameter of the shell, t is the thickness of the shell, f_{y} is the yield value of the shell, $\mathrm{f_d}$ is the design value of the cylinder compressive strength of the slave, $\mathrm{f_k}$ is characteristic compressive strength.

$$\Psi_{\mathrm{cc}} = 0.25(3+2\bar{\lambda}) \le 1 \qquad (9)$$

$$\Psi_s = \left(4.9 - 18.5\bar{\lambda} + \bar{\lambda}^2\right) \ge 0 \qquad (10)$$

$$\bar{\lambda} = \sqrt{\frac{n_{\mathrm{pl,rd}}}{n_{\mathrm{cr}}}} \qquad (11)$$

$$n_{pl,rd} = s_a\ f_a + 0.85\ c_a\ f_d \quad (12)$$

$$(EI)_{eff} = E_s I_f + K_e\ E_m I_o \quad (13)$$

$n_{pl,rd}$ is the characteristic value of the plastic resistance to compression, n_{cr} is the elastic critical normal force for the relevant buckling mode, $(EI)_{eff}$ is effective flexural stiffness, K_e =0.6 is a correction factor, I_f and I_o are the second moments of area of the structural steel section and the uncracked concrete section respectively, E_{cm} is the modulus of elasticity of the uncracked concrete section.

2.2.2. According to the specification of AISC, the design compressive strength, ξP_k, and allowable compressive strength, $P_k/\Omega c$, for axially loaded concrete-filled composite columns shall be determined as;

1. When $P_f \geq 0.44P_o$

$$p_k = p_i[0.685(\frac{p_i}{p_f})] \quad (14)$$

2. When $P_f < 0.44P_i$

$$p_i = 0.877 p_f \quad (15)$$

Where

ξ=0.75 (LRFD) Ωc=2.00(ASD)

$$p_i = s_a f_y + c_2 c_a f_k \quad (16)$$

$$p_f = \pi^2(\frac{IE_{eff}}{(kl)^2}) \quad (17)$$

C_2= 0.95 for circular sections

$$EI_{eff} = E_s I_f + C_3 E_m I_o \quad (18)$$

$$c_3 = 0.6 + 2(\frac{s_a}{c_a + s_a}) \quad (19)$$

$$E_m = w_c^{1.5}\sqrt{f_k} MPa \quad (20)$$

And where S_s is a cross-sectional area of the shell in mm^2, C_a is a cross-sectional area of the slave in mm^2, E_m is the young's modulus of the slave in MPa, E_s is the young's modulus of the shell in MPa, f_k is the compressive strength of slave (MPa), f_y is yield stress of shell in (MPa), I_o is the second moment area of slave in mm^4, I_f is a second-moment area of shell in mm^4, K is the effective length factor, L is laterally unbraced length of the member (mm), W_c is the weight of concrete per unit volume ($1500 \leq W_c \leq 2500$ kg/m^3), $(EI)_{eff}$ is effective stiffness of composite section in (N-mm^2).

2.3. Finite element analysis

The indoor experiment only allows for the observation of the bearing capacity, displacement, strain, and other properties of the axially loaded TCSCFST short columns. Numerical simulation is required to monitor the distribution of axial force and stress in the TCSCFST. In this work, the stress, axial force, and displacement of the TCSCFST, UF, and concrete core with different aspect ratios are investigated using ABAQUS software. A three-dimensional solid element with eight reduced integration nodes (C3D8R) and a shell element with four reduced integration nodes (S4R) are used to simulate the TCSCFST, along with concrete core and UF steel tubes. All degrees of freedom are limited except for the vertical displacement of the loaded top end. The upper end of

the TCSCFST is subjected to a simultaneous compression axial load using vertical displacement control techniques. The interface between the shell and the slave is subject to the tie elements condition, whereas the final specimen is restricted by a rigid body (pin nodes) condition. Several trials are carried out with different mesh sizes and step values (such as step duration, maximum increment, starting increment, minimum increment, and maximum increment size) in order to identify the most suitable mesh and step sizes that would provide reliable and time-efficient results. To track the nonlinear behaviour of the specimens, a nonlinear load-to-displacement analysis phase is added to the Finite Element (FE) modelling procedure. Surface-to-surface contact is the model used to describe the interactions between the slave and shell.

3. Results and Conclusion

3.1. Experimental result

Concrete-filled and unfilled circular section steel tubes with thin wall shells are both investigated in this work. Fig. 3 for M20-6-320-48 specimens shows the experiment's steps and the specimens' manner of failure. The specimens exhibit the three stages of the failure mode classification throughout the experiment. For a certain period of time, referred to as the elastic stage, the load-to-time curve first grows linearly. There are no indications of shell bending or cracking on specimens in the elastic stage. During this phase, the load increases rapidly and linearly with modest axial strain, resulting in a linear connection between strain and load. Furthermore, at this point, the longitudinal strain is larger than the hoop strain for a given load. The curve slows down after its initial linear increase until the load reaches its maximum magnitude. This is the elasto-plastic stage. The specimen reached its maximum load-carrying capacity when the axial load progressively increased during the elasto-plastic stage. In this instance, the longitudinal stress attain maximum while the hoop stress increased progressively beyond the ultimate point. The specimen then begins to bend or crack, and the curve's speed further drops. When the axial strain increased, the curve began to show a downward trend, and the load began to decrease more slowly than it had during the elasto-plastic stage. This third stage is referred to as the plastic stage. The axial strain and hoop strain are now more than the ultimate strain, but there is no sign of fracture. Consequently, the diameter of the outer shell rose considerably. This TCSCFST load-carrying phenomenon explains the columns' improved ductility behaviour in comparison to steel and concrete.

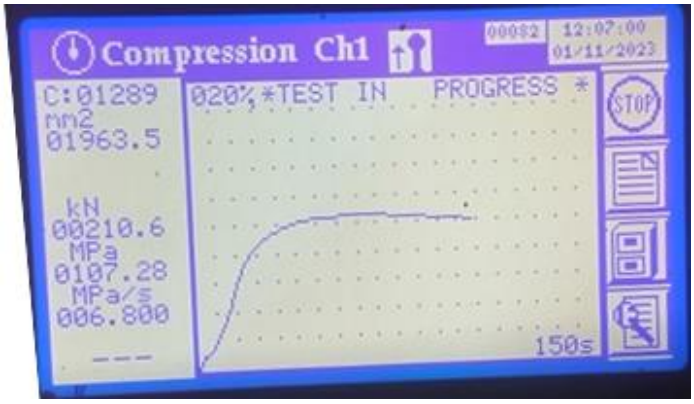

Fig. 3 Compression test result and load-to-time graph of M20-6-320-48 specimen

3.1.1. Axial strength of the TCSCFST and UF

In the experiment, the axial bearing capacity of TCSCFST and UF steel tubes was examined. Compared with the theoretical value, the experimental value of the TCSCFST column showed a significant change in the axial strength. From the result, it is shown that the average load factor of the experimental result of TCSCFST is N_E = 4.92 and N_E = 5.52 from the theoretical value

estimated by Eurocode-4, EN 1994-1-1 (2004) part 1-1 for 320 and 315 mm height specimens, respectively. The experimental result also depicts that the axial bearing capacity of the TCSCFS increased by an average load factor of N_A=4.92 and N_A=5.51 from the theoretical value estimated by AISC design code for 320 and 315 mm height specimens, respectively. In order to know whether the core concrete or shell is highly enhanced by the confinement effect, an investigation of TCSCFS and UF is undertaken. In this investigation, it is also found that the axial load-carrying ability of the core concrete is increasing remarkably compared with the numerical values. When the theoretical value of TCSCFST is determined by Eurocode-4, EN 1994-1-1 (2004) part 1-1, the experiment result shows that the axial strength of core concrete exceeds its axial bearing capacity by an average load factor of N_{CE} = 17.00 and N_{CE} = 21.61 for 320 and 315 mm height specimens, respectively. The experiment also reveals that, compared to the theoretical value calculated using the AISC design code, the core concrete's axial bearing capacity rises by a load factor of N_{CA} = 26.68 and N_{CA} = 34.01 for 320 mm and 315 mm height specimens, respectively. The main reason behind this is because of the shell's confinement effect, which lessened the core concrete's tendency to crush. In addition, the creation of local buckling is prohibited by concrete core. This situation makes the concrete core reach a tri-axial stress state and the shell reach a biaxial stress state. The sharing of stress between the concrete core and the shell is capable enough for the specimen to carry more load. In this study, the specimens are designated with codes. For example, the specimen M20-6-320-48 means M20 denotes the grade of concrete, 6 denotes the sequence of the specimen, 320 denotes the height of the specimen, and 48 denotes the diameter of the specimen. Also on specimens, UF-1-315-48 means UF denotes unfilled steel tubes, 1 denotes the sequence of the specimen, 315 denotes the height of the specimen, and 48 denotes the diameter of the specimen. The experimental, numerical, and load factors of TCSCFS and UF specimens are show in Table 4, 5 and 6.

Table 4 Experimental, numerical, and finite element values of TCSCFST

Designation	Height	P_{exp} (kN)	$P_{u,E}$ (kN)	$P_{u,A}$ (kN)	$P_{u,F}$ (kN)
M20-1-320-48	320	149.2	36.25	37.73	94.33
M20-2-320-48	320	176	36.25	36.27	99.74
M20-3-320-48	320	190.4	36.25	36.27	99.74
M20-4-320-48	320	194.2	36.25	36.27	117.66
M20-5-320-48	320	172.8	36.25	36.27	106.74
M20-6-320-48	320	158.5	36.25	36.27	110.66
M20-7-315-48	315	190.6	36.21	36.27	100.29
M20-8-315-48	315	204.2	36.21	36.27	103.76
M20-9-315-48	315	205.2	36.21	36.27	107.62

Table 5 Experimental, numerical, and finite element load factors of TCSCFST

Specimens	Height	N_E	N_A	N_F	N_{CE}	N_{CA}	$N_{CF,E}$	$N_{CF,A}$

M20-1-320-48	320	4.12	3.95	1.58	10.70	11.23	10.92	11.46
M20-2-320-48	320	4.86	4.85	1.76	16.48	25.87	12.09	18.97
M20-3-320-48	320	5.25	5.25	1.91	19.59	30.75	12.09	18.97
M20-4-320-48	320	5.36	5.35	1.65	20.41	32.04	15.96	25.04
M20-5-320-48	320	4.77	4.76	1.62	15.79	24.79	13.60	21.34
M20-6-320-48	320	4.37	4.37	1.43	12.70	19.94	14.44	22.67
Average		4.92	4.92	1.98	17.00	26.68	13.63	21.40
M20-7-315-48	315	5.26	5.26	1.90	19.81	30.82	12.31	19.16
M20-8-315-48	315	5.64	5.63	1.97	22.77	35.43	13.07	20.33
M20-9-315-48	315	5.67	5.66	1.91	22.99	35.77	13.91	21.64
Average		5.52	5.51	1.93	21.86	34.01	13.10	20.38

Table 6 Experimental, numerical, and finite element value of the UF

Designation	$P_{exp,UF}$ (kN)	$P_{u,UF,E}$ (kN)	$p_{u,UF,A}$ (kN)	$p_{u,UF,F}$ (kN)
UF-1-315-48	101.45	31.62	33.32	43.78
UF-2-315-48	98.5	31.62	33.32	43.78
UF-2-315-48	99.1	31.62	33.32	43.78

3.1.2. Effect of Aspect ratio (L/D) of axial strength of the specimens

In this study, the effect of aspect ratio on the axial strength of TCSCFST for the M20 core concrete, D = 48.17 and T = 1 mm, is examined through experimentation, numerical, and FE analysis methods. As the aspect ratio decreased from 6.64 to 6.54, the average experimental axial bearing capacity of TCSCFST increased by 15.26%. The FE analysis also indicates that the axial bearing capacity of the specimens is reduced by 0.88% when the aspect ratio decreases from 6.64 to 6.54. Furthermore, the numerical result depicts that the average axial bearing capacity of the specimens is almost equivalent in both BS EN 1994-1-1:2004, EN 1994-1-1-11:2004(E) and AISC design code methods when the aspect ratio changes from 6.64 to 6.54. This study uses computational, FE, and experimental approaches to investigate the impact of aspect ratio on the axial strength of TCSCFST for the M20 core concrete, D = 48.17 and T = 1 mm. The average experimental axial bearing capacity of TCSCFST rose by 15.26% as the aspect ratio dropped from 6.64 to 6.54. Additionally, the FE study shows that when the aspect ratio drops from 6.64 to 6.54, the specimens' axial bearing capacity is decreased by 0.88%. Additionally, the numerical result shows that when the aspect ratio shifts from 6.64 to 6.54, the specimens' average axial bearing capacity is nearly equal in both the AISC design code approaches and BS EN 1994-1-1:2004 and EN 1994-1-1-11:2004(E). This demonstrates clearly that the improvement of ductility on TCSCFST specimens causes a significant change in the bearing capacity of the real load-carrying capacity of the TCSCFST short columns with a slight change in aspect ratio. The average experimental, numerical, and FE analysis values with respect to aspect ratio are shown in Table 7.

Table 7 Experimental and numerical value of specimen on different aspect ratio

Grade of concrete	Aspect ratio	$P_{exp.}$	$P_{u,EC}$	P_{AISC}	P_{FE}
M20	6.64	173.52	36.25	36.27	104.81
	6.54	200.00	36.21	36.27	103.89
% decreased		15.26	-0.11	0.00	-0.88

3.1.3. Failure mode

All 12 samples in this experiment failed due to global bending, local buckling, and cracks. The shell's junction is where the cracks are formed. Global buckling occur in single and double curvature, while local buckling involves swelling outward. Three of the nine TCSCFST specimens fail with global buckling, and six fail with cracking. As seen in Fig. 4, all three of the unfilled examples fail due to local buckling, which causes them to bulge outward at the top and bottom.This shows that the presence of slaves in the steel tube prevents local buckling from forming in the filled circular steel tubes, causing cracking and global buckling as the failure modes. This improves TCSCFS's ductility behavior and raises the specimens' axial bearing capacity. The specimen decreases height longitudinally and grows width laterally when the vertical force is operational. The TCSCFS shell experiences lateral tension during this event, which causes the slave's lateral stress to result in the creation of proof stress on the shell. In addition to causing longitudinal cracks on the shell, this proof stress causes the cross-sectional expansion of the shell, as shown in Fig 5. Local and global buckling appeared after the elastic range in the concrete-filled steel tubes, followed by concrete crushing.

Fig. 4 Failure mode of unfilled steel tubes

a) Global buckling b) Global buckling and cracking at bottom
c) Local buckling and cracking at the middle
Fig. 5 Different failure modes of TCSCFST

3.2. Finite element result

Using ABAQUS software, the study's experimental outcome was verified using the FE approach. The load to deformation data and accompanying curves for TCSCFST, UF steel tube, and concrete core were supplied by the FE results. Figure 6 displays the TCSCFST peak loads from numerical, experimental, and FE models. The FE analysis techniques are also used to verify the experimental findings. The comparison reveals that the axial bearing capacity of the TCSCFS investigated by the experiment surpasses by the load factor of N_F = 1.98 and N_F = 1.93 for specimens with heights of 320 and 315 mm, respectively, based on the FE result. A FE analysis investigation on TCSCFS and UF steel tube is conducted to determine whether a core concrete or shell is greatly boosted by the confinement effect. The results of the FE analysis indicate that, in comparison to the numerical value determined by Eurocode-4, EN 1994-1-1 (2004) part 1-1, the axial bearing capacity of the core concrete is improved by a load factor of $N_{CF,E}$ = 13.63 and $N_{CF,E}$ = 13.10 for specimens that are 320 and 315 mm high, respectively. Furthermore, compared to the numerical value calculated by AISC, the axial bearing capacity of the core concrete as determined by FE analysis also rose by a load factor of $N_{CF,A}$ = 21.40 and $N_{CF,A}$ = 20.38 for specimens with heights of 320 and 315 mm, respectively. Additionally, the FE study shows that when the aspect ratio drops from 6.64 to 6.54, the specimens' axial bearing capacity is decreased by 0.88%. The axial bearing capacity values and load factors are shown in Table 4, 5 and 6. The relationship between load and displacement for TCSCFST, UF, and concrete core modelling is also shown in Fig.7 and 8. Fig.7 show a load to displacement curve of TCSCFST, core concrete and UF steel tubes for M20-4-320-48 for 320 mm high specimen whereas Fig. 8 show TCSCFST, core concrete and UF steel tubes for 320 and 315 mm height specimens. From the Figures, the load-to-displacement curve of the UF specimen attains its yield point early and decreases sharply after reaching its yield point compared to TCSCFST and core concrete specimens. This depicted that the vertical load strength of unfilled steel tubes is weak compared with TCSCFST and slave. Likewise from the fig, the load-to-displacement curve of the M20 core concrete specimen decreases downward after reaching its

yield point with a better parabolic shape curve than UF steel tube specimens with small displacement values. This indicates that even though the vertical load resistance of the slave is better than the UF specimens, its ductility behavior is weak compared to UF steel tubes. The load-to-displacement curve of the TCSCFS specimens in the figure also demonstrates that, once it reached its yielding point, it decreased with a better parabolic shape and a displacement value that was higher than that of core concrete but lower than that of UF steel tubes. This illustrates that TCSCFS exhibits higher ductility behavior than core concrete and lower ductility behavior than UF steel tube. Consequently, a greater axial load may be supported by TCSCFS specimens than by UF steel tubes and core concrete. This is because the slave is constrained by the outer steel and the shell is constrained by the core concrete. Therefore, the presence of the shell reduces the crushing behavior of the concrete, while the presence of the core concrete prevents the production of local buckling. This interaction of steel and core concrete increased the mechanical behavior of TCSCFS, such as yield point, strength, toughness, and elasticity compared with unfilled steel tubes and concrete core. Figures 9, 10, and 11 display the failure mode of M20-4-320-48 specimen when the specimen is unfilled, only core concrete and when the specimen is filled with concrete, respectively. The failure mode in the UF steel tube simulation demonstrated the development of local buckling at the top where load was applied and at the bottom where reaction force was present. Von Mesis stress value and axial displacement of the FE modelling for M20-4-320-48 TCSCFST, UF steel tube, and core concrete, respectively. The figures show that the specimens' tops have the highest displacement and Von Mesis stress values represented by red, while their bottoms have the lowest displacement and Von Mesis stress values indicated by blue.

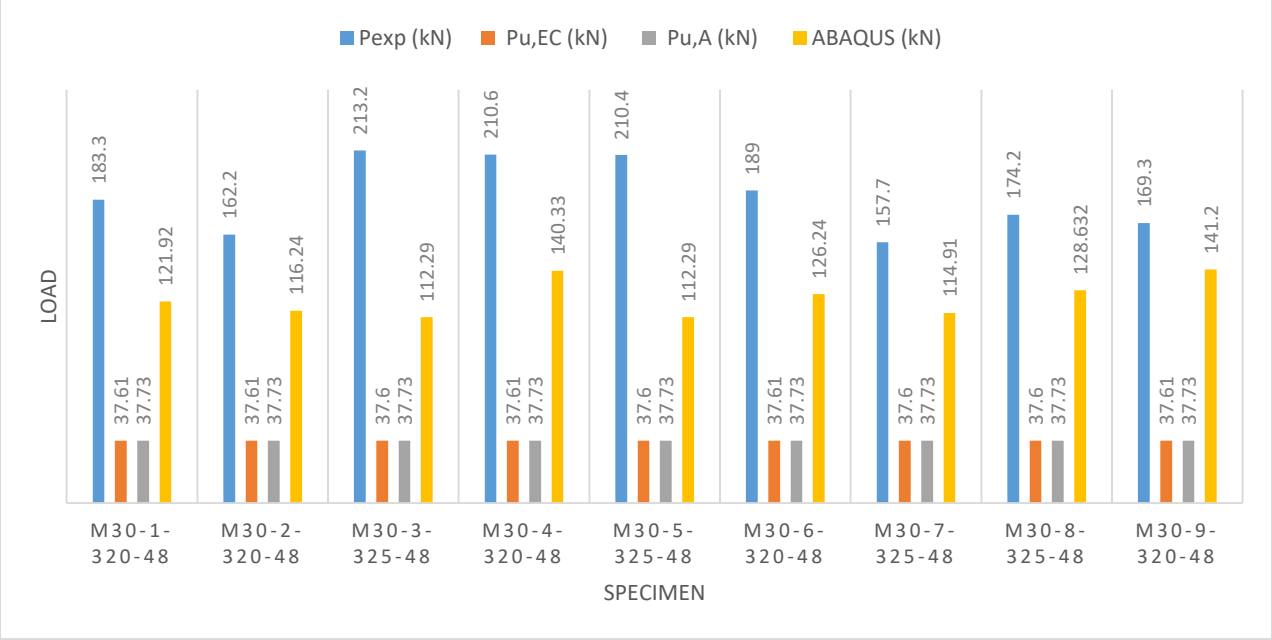

Fig. 6 Average experimental, numerical, and FE values of TCSCFST

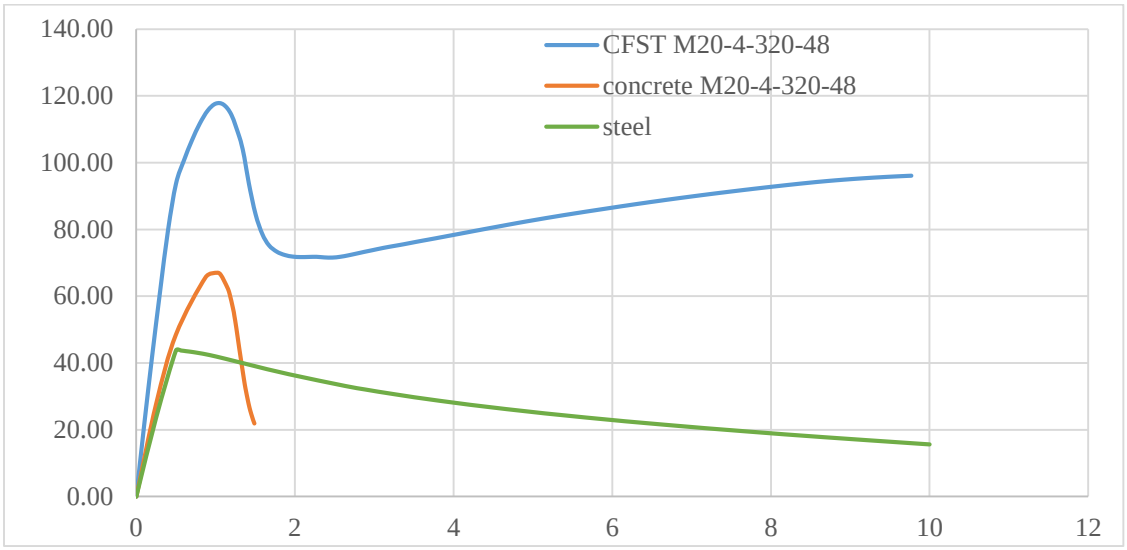

Fig. 7 Load-to-displacement graph for TCSCFST, UF, and concrete core for M20-4-320-48 specimens

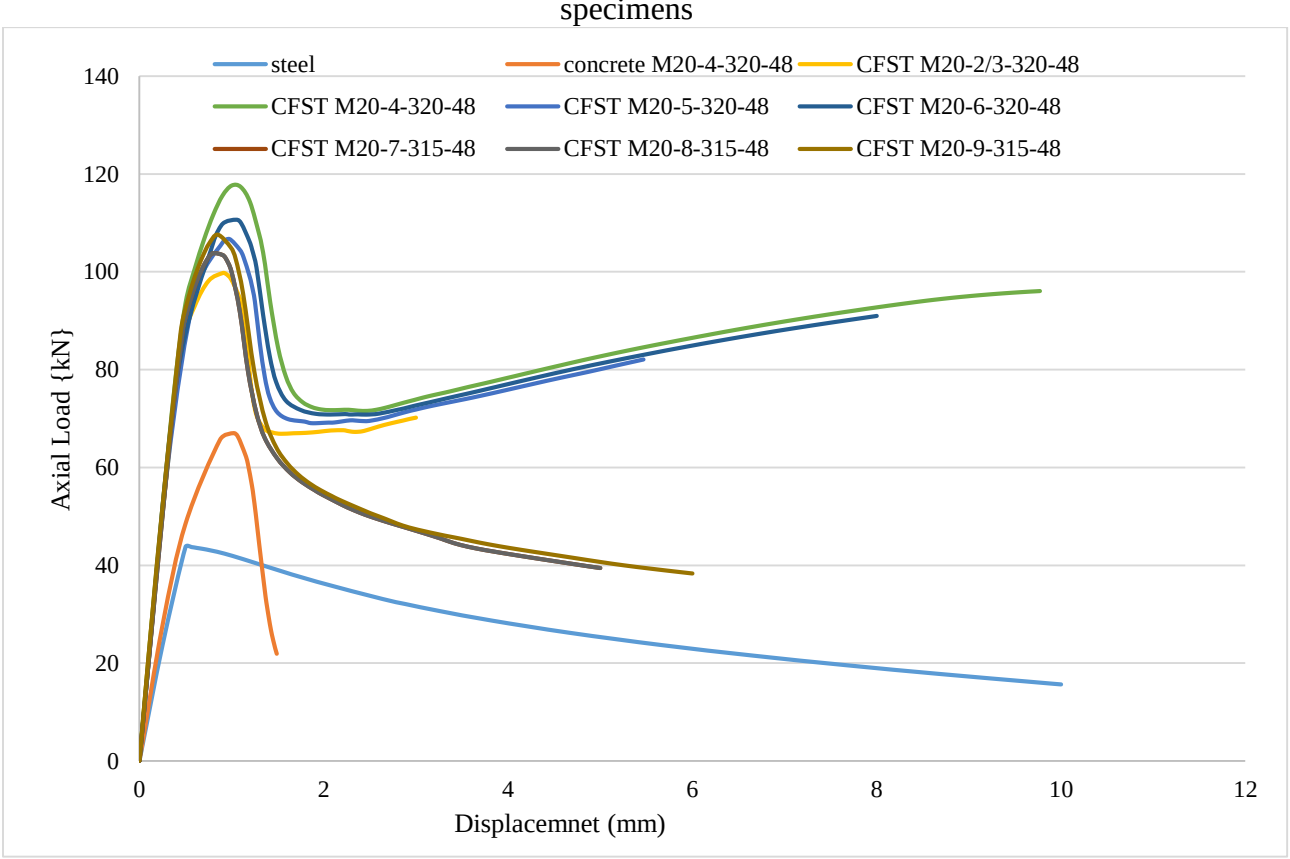

Fig. 8 Average experimental, numerical, and FE values of TCSCFST

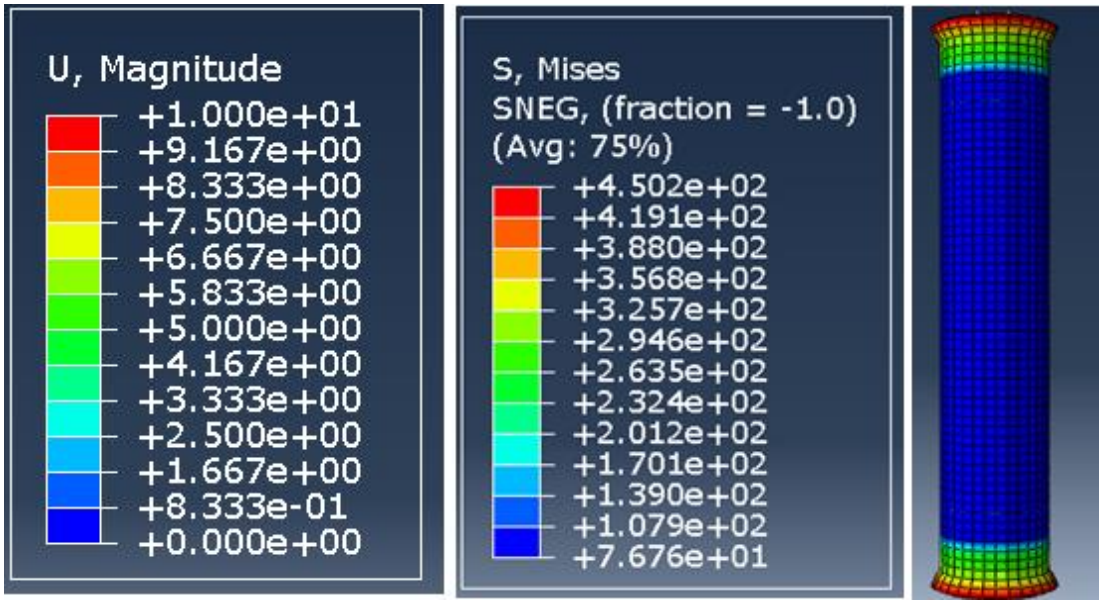

Fig. 9 Failure mode of shell (M30-4-325-48) by FE analysis

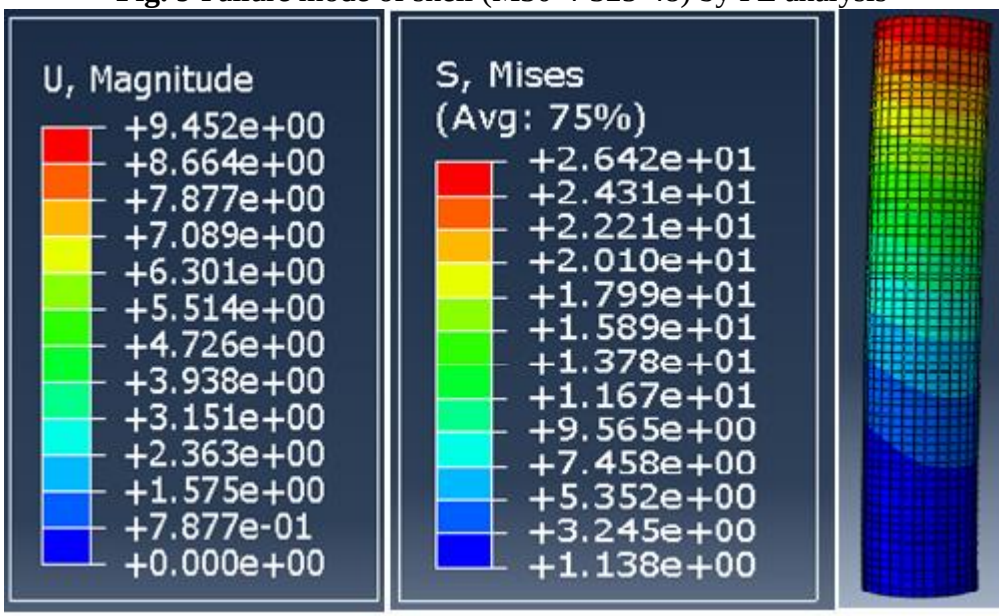

Fig. 10 Failure mode of concrete (M30-4-325-48 specimen) by FE analysis

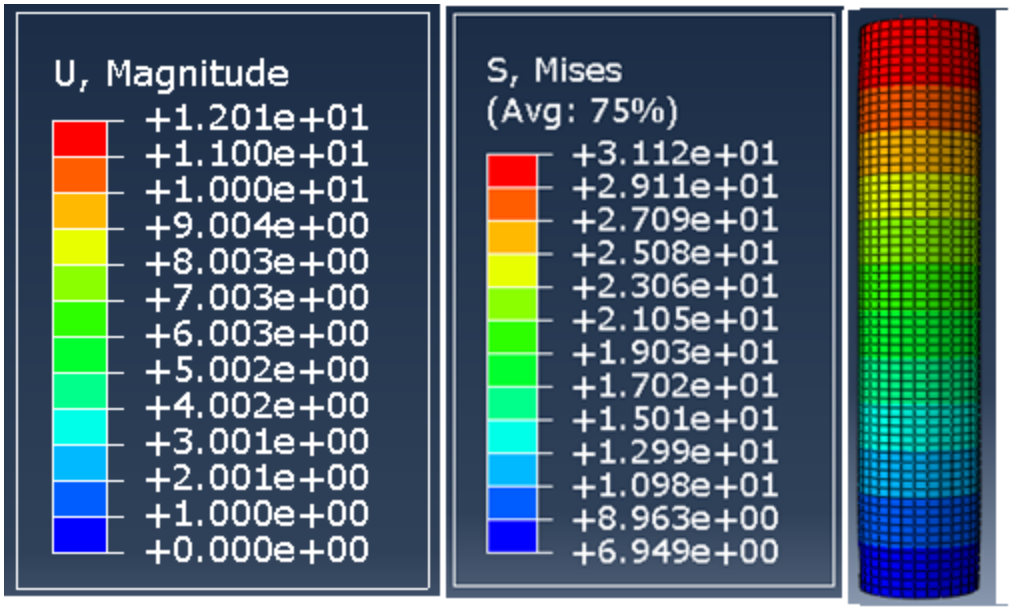

Fig. 11 Failure mode of TCSCFST (M30-4-325-48 specimens) by FE analysis

3.2. Conclusion

In the study, the experimental outcomes, the theoretical value, and the finite element analysis of TCSCFST, UF, and slave specimens were surveyed. The variables considered during the study are M20 core concretes, aspect ratio, a numerical value estimated by Eurocode-4, EN 1994-1-1 (2004), and a numerical value estimated by AISC. Uniaxial loading is applied for nine TCSCFST and three UF steel tubes. When the numerical values of TCSCFST and core concrete are compared with the experimental and FE modeling outcomes, numerical values are smaller and highly conservative. Filling concrete inside the shell prohibits the failure of the steel tube or shell by local buckling, and confining concrete with steel resist the crushing behavior of core concrete. The effect of the variables on the axial bearing capacity, load-to-deformation relationship, failure mode, and FE modeling results are discussed. Finally, the following conclusions are drawn:

1. The average load factor of the experimental result of TCSCFST is N_E =4.92 and N_E =5.52 from the theoretical value estimated by Eurocode-4, EN 1994-1-1 (2004) part 1-1 for 320 and 315 mm height specimens, respectively, and The experimental result also depicts that the axial bearing capacity of the TCSCFS increased by an average load factor of N_A=4.92 and N_A=5.51 from the theoretical value estimated by AISC design code for 320 and 315 mm height specimens, respectively.
2. When the theoretical value of TCSCFST is determined by Eurocode-4, EN 1994-1-1 (2004) part 1-1, the experiment result shows that the axial strength of core concrete exceeds its axial bearing capacity by an average load factor of N_{CE} =17.00 and N_{CE} =21.61 for 320 and 315 mm height specimens, respectively. The experiment also reveals that, compared to the theoretical value calculated using the AISC design code, the core concrete's axial bearing capacity rises by a load factor of N_{CA} =26.68 and N_{CA} =34.01 for 320 mm and 315 mm height specimens, respectively.
3. When the aspect ratio decreased from 6.64 to 6.54, the average experimental axial bearing capacity of TCSCFST increased by 15.26%. The FE analysis also indicate that the axial bearing capacity of the specimens is reduced by 0.88% when the aspect ratio decrease from 6.64 to 6.54. This clearly shows that a small change in aspect ratio results in a considerable bearing capacity change on the actual load-carrying capacity of the TWCSCFST short columns as a result of the enhancement of ductility on TWCSCFST specimens.

4. The failure mode of TCSCFST during testing is via cracking and global buckling, while the mode of failure of the UF steel tube was via local bucking; this is due to the confinement effect of the shell.
5. The axial bearing capacity of TCSCFS examined by experiment exceeds by the load factor of N_F=1.98 and N_F=1.93 for 320 and 315 mm height specimens, respectively, from the FE result.
6. The FE analysis result show that the axial bearing capacity of the core concrete increased by a load factor of $N_{CF,E}$ =13.63 and $N_{CF,E}$ = 13.10 for 320 and 315 mm height specimens, respectively, from the numerical value estimated by Eurocode-4, EN 1994-1-1 (2004) part 1-1 and the axial bearing capacity of the core concrete determined by FE analysis also increased by a load factor of $N_{CF,A}$ =21.40 and $N_{CF,,A}$ = 20.38 for 320 and 315 mm height specimens, respectively, from the numerical value estimated by AISC.

References

[1] X. Yan, H. Wenhui, M. Xiaoyong, C. Kang-kyu and Z. Pingsheng, "Confinment design of CFT columns for improved sesmic performance".

[2] A. K. H. Kwan and Y. Ouyang, "A Novel Finite Element Method for Analysing the Confinement Effect in Concrete-Filled Steel Tubes,," Journal of Civil Engineering Research, vol. 7, no. 2, pp. 57-62, 2017.

[3] A. A. Ali and N. J. Abbas, "Behavior of Box Concrete Filled Steel Tube Columns Considering Confinement Effect,," International Journal of Steel Structures, vol. 21, no. 3, p. 950–968, (2021).

[4] J. Cai and Y.-L. Long, "Axial Load Behavior of Rectangular CFT Stub Columns with Binding Bars," Advances in Structural Engineering, vol. 10, no. 5, 2007.

[5] L.-H. Han, W. Liu and Y.-F. Yang, "Behavior of thin-walled steel tube confined concrete stub columns subjected to axial local compression,," Thin-Walled Structures, vol. 46, p. 155–164, 2008.

[6] Y. Xiao, W. He and K.-k. Choi, "Confined Concrete-Filled Tubular Column," Journal of structural engineering, vol. 131, pp. 488-497, 2005.

[7] A. A. Ali and N. J. Abbas, "Behavior of Box Concrete Filled Steel Tube Columns Considering Confinement Effect," International Journal of Steel Structures, vol. 21, no. 3, p. 950–968, 2021.

[8] H. A. Le, "Evaluation of Confining Pressure Models for Circular Concrete-Filled Steel Tube Short Columns under Concentric Loading," Engineering, Technology & Applied Science Research, vol. 13, no. 1, pp. 10181-10185, 2023.

[9] L. He, Y. Zhao and S. Lin, "Experimental study on axially compressed circular CFST columns with improved confinement effect," Journal of Constructional Steel Research, 2017.

[10] Z.-w. Yua, F.-x. Dinga and C. Caib, "Experimental behavior of circular concrete-filled steel tube stub columns," Journal of Constructional Steel Research, vol. 63, p. 165–174, 2007.

[11] B. L. Bing, R. Park and H. Tanaka, "Stress-Strain Behavior of High-Strength Concrete Confined by Ultra-High- and Normal-Strength Transverse Reinforcements," ACI Structural Journal, 2001.

[12] F. Abed, M. AlHamaydeh and S. Abdalla, "Experimental and numerical investigations of the compressive behavior of concrete filled steel tubes," Journal of Constructional Steel Research, 2012.

[13] Z. Tao, L.-H. Han, B. Uy and X. Chen, "Post-fire bond between the steel tube and concrete in concrete-filled steel tubular columns," Journal of Constructional Steel Research, no. 67, p. 484–496, 2011.

[14] Liang and Q. Quan, "Nonlinear analysis of circular double-skin concrete-filled steel tubular columns under axial compression," Engineering Structures, vol. 131, pp. pp. 639-650. ISSN 0141-0296, 2017.

[15] Y. du, Z. Chen, C. Zhang and X. Cao, "Research on axial bearing capacity of rectangular concrete-filled steel tubular columns based on artificial neural networks," Front. comput. sci., vol. 11, no. 5, p. 863–873, 2017.

[16] IS1608:2005, "Metallic materials - tensile testing at ambient temperature," Bureau of Indian standards, 2005.

[17] IS10262:2019:, "Indian Standard, Concrete Mix Proportioning-guidline," Bureau of Indian standards, 2019.

[18] EN1994-1-1:2004, "Design of composite steel and concrete structures – Part 1-1. General rules and rules for buildings," The European Union, 2004.

[19] ANSI/AISC-360-16, "Specification for structural steel building," in An American National Standard, Chicago, American Institute of Steel Construction, 2016.